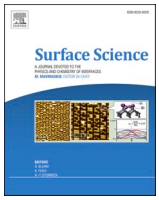
Surface Science 749 (2024) 122565



Contents lists available at ScienceDirect

Surface Science

journal homepage: www.elsevier.com/locate/susc





Using Auger transitions as a route to determine the oxidation state of copper in high-pressure electron spectroscopy

Markus Soldemo [a,1,*], Fernando Garcia-Martinez [c], Christopher M Goodwin [b,2], Patrick Lömker [b], Mikhail Shipilin [c], Anders Nilsson [b], Peter Amann [d], Sarp Kaya [e], Jonas Weissenrieder [f,*]

[a] PULSE Institute, SLAC National Accelerator Laboratory, Menlo Park, CA 94025, USA
[b] Department of Physics, Stockholm University, SE-10691 Stockholm, Sweden
[c] Photon Science, Deutsches Elektronen-Synchrotron DESY, Notkestr. 85, 22607 Hamburg, Germany
[d] Scienta Omicron AB, Danmarksgatan 22, 75323 Uppsala, Sweden
[e] Department of Chemistry, Koç University Tüpraş Energy Center (KUTEM), Koç University, 34450 Istanbul, Türkiye
[f] Materials and Nano Physics, School of Engineering Sciences, KTH Royal Institute of Technology, SE-100 44 Stockholm, Sweden

ARTICLE INFO

Keywords:
High pressure XPS
Auger electron spectroscopy
Copper
Oxidation state
Heterogeneous catalysis

ABSTRACT

Accurate discrimination between metallic copper (Cu^0) and cuprous oxide (Cu_2O, Cu^+) in electron spectroscopy commonly relies on the Auger electron spectroscopy (AES) Cu $L_3M_{4,5}M_{4,5}$ transitions, as the X-ray photoelectron spectroscopy (XPS) Cu core-levels do not provide large enough binding energy shifts. The kinetic energy of the AES Cu $L_3M_{4,5}M_{4,5}$ electrons is ~917 eV, which leaves the AES electron susceptible for efficient scattering in the gas phase and attenuation of the signal above near-ambient pressure conditions. To study copper-based materials at higher pressures, e.g., the active state of a catalyst, Auger transitions providing electrons with higher kinetic energies are needed.

This study focuses on AES transitions involving the Cu K-shell (1s electrons) that exhibit discernible kinetic energy shifts between the oxidation states of Cu. It is shown that the AES Cu $KL_2M_{4,5}$ transition, with kinetic energy of ~7936 eV, provides a large enough kinetic energy shift between metallic copper and Cu_2O. AES signal is demonstrated in an ambient of 150 mbar CO_2.

1. Introduction

Copper oxide and copper oxide derived catalysts show catalytic activity towards industrial relevant reactions, such as CO oxidation [1], CO_2 hydrogenation reactions [2,3], epoxidation reactions [4-6], and photocatalytic water splitting [7]. The catalytic activity is often linked to a specific oxidation state, stabilizing the active oxidation state is a key strategy against catalyst deactivation. Therefore, the ability to accurately determining the active site's oxidation state in *operando* studies is important for understanding catalysis. For example, the active site for the CO oxidation reaction over copper oxide based catalysts is Cu^+ (Cu_2O) but not Cu^{2+} (CuO) nor Cu^0 (metallic copper) [8]. Electron spectroscopy methods, such as X-ray photoelectron spectroscopy (XPS) and Auger electron spectroscopy (AES), have proven to be invaluable tools to acquire insight into how catalysis proceed on model system surfaces [9]. The kinetic energy of the emitted photoelectrons in XPS depends on the photon energy whereas the kinetic energy for the Auger electrons in AES depend on the Auger decay channel. In contrast to ultra-high vacuum conditions, at high-pressure conditions, the electrons must travel through a gas between the specimen and the analyzer. The electrons scatter in gas, the gas phase scattering is kinetic energy dependent and generally higher electron kinetic energy leads to lower scattering probability. The electron scattering processes in the gas phase attenuate the signal and at high gas pressures the signal may be fully attenuated. In XPS, a change in oxidation state often results in a significant binding energy shift of core-levels. For copper, this chemical shift is too small for an unambiguous discrimination of Cu^0 and Cu^+. At near-ambient pressure (NAP) conditions, up to gas pressures of a few

* Corresponding authors.
E-mail addresses: markus.soldemo@fysik.su.se (M. Soldemo), jonas@kth.se (J. Weissenrieder).
[1] Present address: Department of Physics, Stockholm University, SE 106 91 Stockholm, Sweden.
[2] Present address: ALBA Synchrotron Light Facility, Carrerde la Llum 2, 26, 08290 Cerdanyola del Vallés, Spain.

https://doi.org/10.1016/j.susc.2024.122565
Received 28 May 2024; Received in revised form 16 July 2024; Accepted 22 July 2024
Available online 26 July 2024
0039-6028/© 2024 The Authors. Published by Elsevier B.V. This is an open access article under the CC BY license (http://creativecommons.org/licenses/by/4.0/).

mbar, the AES lines of Cu $L_3M_{4,5}M_{4,5}$ are routinely employed to discriminate between Cu^0 and Cu^+ due to the significant kinetic energy shift, see examples of studies in refs [10–15]. The peak assignment of the AES Cu $L_3M_{4,5}M_{4,5}$ region was discussed by Pauly et al [16]. The low kinetic energy of Cu $L_3M_{4,5}M_{4,5}$, around 914 eV, leaves the electrons susceptible to efficient scattering in the gas-phase, which prevents *operando* studies at higher pressure conditions.

Using hard X-rays, it is possible to perform electron spectroscopy studies involving the Cu 1s core-level (K-shell). With the two Mo Kα X-ray energies and an electron kinetic energy analyzer, Nordling *et al.* determined the binding energy of Cu 1s from a copper film to ~8985.5 eV [17]. Lee et al. reported the kinetic energies and relative intensities for AES transitions involving the K-shell of Cu, the kinetic energies of the peak intensity in the KLL, KLM, and KMM regions are 7.1 keV, 7.9 keV, and 8.8 keV, respectively, and the peak intensities, normalized to the background signal at the high kinetic energy side of Cu KMM region are 30, 12, and 2 for Cu KLL, KLM, and KMM, respectively [18]. A detailed Auger decay channel assignment of the peaks for AES Cu KLM and Cu KLN regions was done by Inoyatov et al. [19] and for the AES Cu KLL region was reported by Went and Vos [20] and by Ergi et al. [21].

The facile reduction ($Cu/Cu_2O(100)$) and oxidation ($CuO/Cu_2O(100)$) nature of the $Cu_2O(100)$ surface can be utilized as a benchmark for the identification of the Cu oxidation state at *operando* conditions. The surface structure of $Cu_2O(100)$ in UHV has been subjected to numerous studies, see e.g. [22–24]. Schulz and Cox studied the interaction of hydrogen gas (H_2) with $Cu_2O(100)$ at UHV conditions and found no dissociative adsorption [25]. Tissot et al. studied the reduction of $Cu_2O(100)$ and $Cu_2O(111)$ by the interaction of atomic hydrogen at UHV conditions, they showed OH-group formation at room temperature and reduction into metallic clusters at the surface at elevated temperatures [26]. At H_2 pressures in the mbar regime at 800 °C, Ramanarayanan and Alonzo found Cu_2O is reduced [27]. A slow reduction process of $Cu_2O(100)$ in H_2 gas can work as model system to monitor and compare the transition from Cu^+ to Cu^0 using different Auger transitions.

This study focuses on how to discern the oxidation state of copper at high pressure conditions (pressures higher than common near-ambient pressure conditions) using XPS and AES involving the Cu 1s core-level. Similar to the shallower copper core-levels in XPS, no binding energy shift is observed that permits discriminating Cu° from Cu^+. In the AES Cu KLM region, the Cu $KL_2M_{4,5}$ transition is found to carry similar kinetic energy shifts between the different oxidation states as the Cu $L_3M_{4,5}M_{4,5}$ transition . This Auger transition provides electrons with kinetic energy of ~7936 eV and thus enables the discrimination between Cu_2O and Cu at higher pressure conditions. To compare the AES Cu $L_3M_{4,5}M_{4,5}$ and Cu $KL_2M_{4,5}$ transitions, they are alternatingly measured during *in-situ* reduction of $Cu_2O(100)$ to $Cu/Cu_2O(100)$ in 75 mbar H_2 at 80 °C. The signal attenuations for the two AES transitions were compared in 150 mbar CO_2 environment, a relevant gas for e.g. catalytic CO_2 reduction reaction studies, showing the Cu $KL_2M_{4,5}$ transition provided a clear signal while the Cu $L_3M_{4,5}M_{4,5}$ transition was fully attenuated.

2. Experimental details

The experiments were carried out using the POLARIS high-pressure XPS endstation [28] at the P22 beamline [29] of the Petra III synchrotron radiation facility at DESY in Hamburg, Germany. The POLARIS system permits *operando* hard X-ray electron spectroscopy studies up to pressures above 1 bar [28]. The POLARIS instrument is equipped with a differentially pumped Scienta Omicron R4000-Hipp-2 electron analyzer with a custom designed front cone. The high gas pressure environment at the surface is achieved by creating a virtual gas cell between the sample surface and the electron analyzer's front cone from which the gas flow. It is not possible to maintain this virtual gas cell if grazing the sample relative the analyzer.. The photon energy of the X-ray light was 9800 eV and was linear polarized perpendicular to the surface plane. The X-ray incidence grazing angle was 0.4°, which provides an estimated X-ray attenuation length along the surface normal direction of ~42 nm [30]. The POLARIS system is equipped with sample preparation equipment, such as sample heater, argon ion sputter gun, and high-precision leak-valves for gas dosing. The sample temperature was monitored via type N thermocouple in contact with the backside of the sample.

The $Cu_2O(100)$ specimen is a natural crystal acquired from a commercial manufacturer (Surface Preparation Laboratories, the Netherlands), its surface is mirror polished and aligned within 0.1°. Initial sample degassing and surface cleaning were conducted in a separate UHV system and the surface was checked by low energy electron diffraction (LEED). In the POLARIS instrument, the surface is cleaned by cycles of argon ion sputtering and subsequent annealing in an oxygen gas atmosphere. The procedure is known to produce a well-reproducible LEED-pattern [23,31].

The XPS binding energy scales reported in this work are corrected to the known binding energy of Cu $2p_{3/2}$ for $Cu_2O(100)$ from soft X-ray photoelectron spectroscopy, see e.g., [32], no corrections for the electron emission recoil effect were applied. The kinetic energies for AES spectra are reported as measured. All presented XPS data are intensity normalized on the low binding energy side of the core-level region and all AES data at the high kinetic energy side of the region. The XPS data is peak fitted using the FitXPS version 3 software that has implemented Doniach-Sunjic line shapes convoluted with Gaussian line shapes for experimental broadening. Shirley backgrounds were removed using the Fityk 1.3.1 software prior peak fitting.

3. Experimental results and discussion

3.1. Core-level photoelectron spectroscopy

The XPS core-level measurements were performed in high-vacuum conditions using X-rays with photon energy of 9800 eV. The XPS core-level spectra of the Cu 1s and O 1s regions for three different oxidation states of copper ($CuO/Cu_2O(100)$ (Cu^{2+}), $Cu_2O(100)$ (Cu^+), and $Cu/Cu_2O(100)$ (Cu^0)) are presented in Fig. 1. The oxidation state of copper for each surface was controlled using the AES Cu LMM region (AES is discussed in later section). In this study, the kinetic energy of the XPS Cu 1s photoelectrons is approximately 820 eV, compared to 915 eV for AES Cu LMM. This means the probing depth for the AES Cu LMM and XPS Cu 1s are comparable, which allows for proper oxidation state assignment of peaks in XPS Cu 1s from the corresponding AES Cu LMM spectrum.

Comparing the XPS Cu 1s core-level spectra for $Cu_2O(100)$ and $Cu/Cu_2O(100)$ (Fig. 1(a)), it is apparent that their binding energies overlap. In fact, the two spectra were peak fitted using the same parameters except for the peak intensity. The binding energy of Cu 1s for metallic copper is here determined to be 8979.4 eV, compared to ~8985 eV as reported by Nordling et al. [17]. The lack of binding energy shift in Cu 1s between $Cu_2O(100)$ and $Cu/Cu_2O(100)$ makes it impossible to discern the two oxidation states by using the core-level, which follows the behavior of the shallower core-levels such as the Cu 2p core-level. The CuO component for $CuO/Cu_2O(100)$ in XPS Cu 1s is, on the other hand, shifted by 1.5 eV towards higher binding energies relative to the Cu_2O component. A minor binding energy shift of ~−0.05 eV is noticed for the Cu_2O peak for the $CuO/Cu_2O(100)$ surface compared to pristine Cu_2O (100), which is within the expected experimental resolution. The $CuO/Cu_2O(100)$ surface also features a strong additional peak that is located at ~7.4 eV to higher binding energies of the main CuO component. This binding energy shift is similar to what has been reported for shallower Cu core-levels of CuO and it has been suggested to originate from core ionization induced electron transfer from O 2p to Cu 3d states via the Cu 4sp-band [33]. High binding energy components in the 1s core-level for other 3d transition metals have been reported.

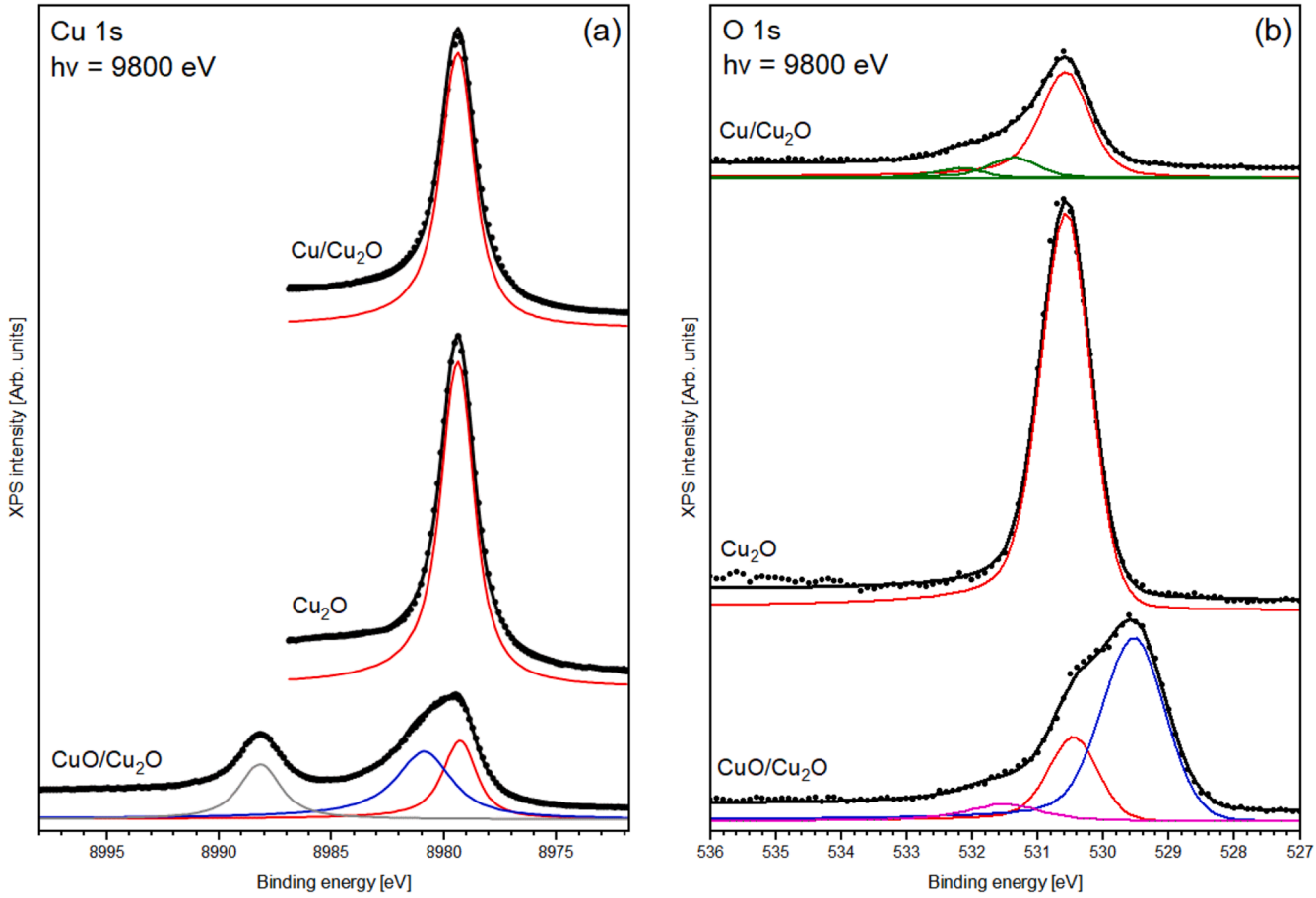


Fig. 1. XPS recorded at hv = 9800 eV of the core-levels (a) Cu 1s and (b) O 1s at different oxidation states. Each spectrum is normalized on the low binding energy side of each region. Red: Cu_2O (and metallic Cu for Cu 1s in (a)). Blue: CuO. Gray: Charge transfer final state peak for CuO. Green: Subsurface oxygen in reduced copper. Magenta: OH-species.

Miedema et al. reported and discussed charge transfer peaks in HAXPES Fe 1s for Fe_2O_3 [34]. For Ni, Karis et al. studied the binding energy shifts of the multiplet peak for different core-levels, they showed that the binding energy shift is lower for deeper core-levels [35]. As the binding energy shift for the high binding energy component in Cu 1s for CuO is similar to what has been reported for the shallower core-levels, this component is therefore here suggested to not originate from core-hole interaction with a multiplet final state.

The XPS O 1s spectra in Fig. 1(b) for the three surfaces follow the pattern observed in Cu 1s. The spectrum for the $Cu_2O(100)$ surface does not feature a component for under-coordinated surface oxygen atoms as a shoulder on the low-binding energy side of the main peak, which commonly is resolved in soft X-ray photoelectron spectroscopy [23,36]. The reason is a combination of the lower instrument resolution that broadens the contribution and the deeper probing depth that gives higher relative intensity to the bulk Cu_2O component. The spectrum for the $Cu/Cu_2O(100)$ surface shows reduced intensity compared to that of $Cu_2O(100)$. Peak fitting the reduced surface requires components for the high-binding energy contribution, this follows what is reported by Wang et al. [37] for subsurface oxygen in oxide-derived copper. For the oxidized surface, $CuO/Cu_2O(100)$, two contributions are visually present. The CuO component is shifted towards lower binding energies relative to the peak for the $Cu_2O(100)$ surface. The parameters used for peak fitting the Cu_2O component was locked to those used for pristine $Cu_2O(100)$ but with the same binding energy shift of 0.05 eV added to lower binding energies as was observed in Cu 1s. The peak fitting finds the CuO component shifted 0.93 eV to lower binding energy relative the Cu_2O component. This is close to the by Wang et al. reported 1 eV shift towards lower binding energy in O 1s when oxidizing $Cu_2O(100)$ into CuO at 0.1 mbar O_2 gas pressure [32]. There is also a small signal contribution at ~1.05 eV to higher binding energies of the Cu_2O component. This shift matches the hydroxylation O 1s component in literature, rather than water adsorbate that is reported at a higher binding energy shift [26,32,38]. This component is likely originating from water in the background pressure in the experimental chamber.

3.2. *Auger electron spectroscopy*

For using an Auger transition to discern metallic Cu from Cu_2O at high pressure conditions, its signal must be strong enough. This is dependent on (i) the probability for the Auger transition (initial intensity) and (ii) the scattering in the gas phase. The second requirement necessitates that the electrons possess sufficiently high kinetic energy to achieve a long enough inelastic mean-free path in the gas phase. This requirement is not fulfilled by the Cu LMM transitions, that routinely is used at NAP-XPS instruments with pressures up to around 1 mbar regime. Auger transitions involving the K-shell (i.e., the KLL-, KLM-, and KMM-transitions) provides electrons with higher kinetic energy than the LMM-transitions. Lee *et al.* [18] studied the relative signal intensities for these Cu Auger transitions. Their results show that the peak intensity of Cu KLM and Cu KMM are about 40% and 7.5% of the Cu KLL peak intensity, respectively. This suggests the Cu KMM transitions will provide insufficient signal at higher pressures. To examine which Auger transitions that provide sufficient AES signal at gas conditions relevant for model catalysis studies, Fig. 2 compares the AES Cu LMM, Cu KLL, and Cu KLM regions from the clean stoichiometric $Cu_2O(100)$ measured at a

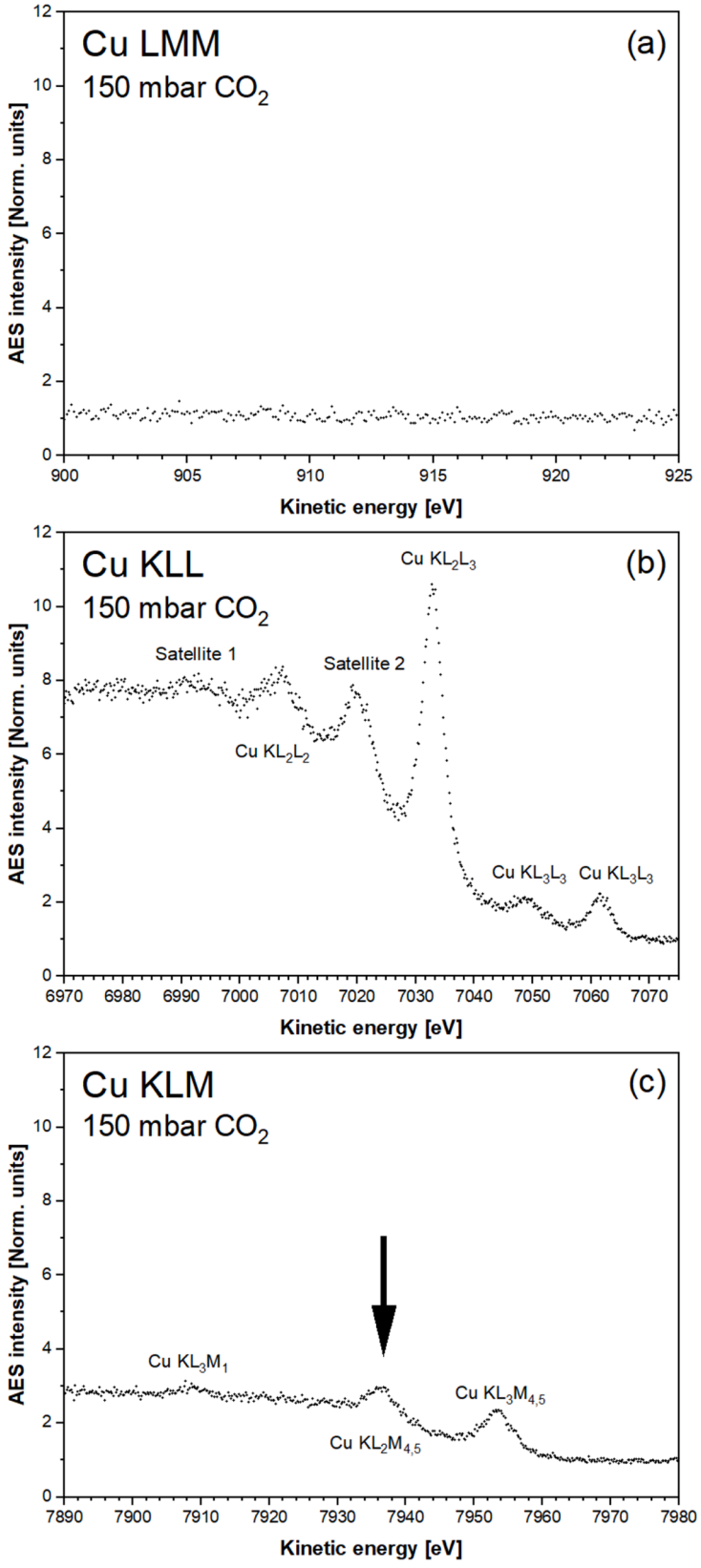


Fig. 2. Auger electron spectra from clean stoichiometric $Cu_2O(100)$ at (a) Cu LMM, (b) Cu KLL, and (c) Cu KLM regions in 150 mbar CO_2. The arrow in (c) indicates the Cu $KL_2M_{4,5}$ peak, which features the strongest energy shift between Cu^0 and Cu^+. All regions are normalized to the background on the low kinetic energy side and presented on the same intensity scale for comparison.

gas pressure of 150 mbar CO_2. All spectra are normalized to the background intensity at the high kinetic energy side in each region and are presented on the same normalized intensity scale for comparison. Fig. 2 (a) shows that the Auger electrons from the Cu LMM transitions are fully attenuated by the inelastic scattering in the gas while both Cu KLL (Fig. 2 (b)) and Cu KLM (Fig. 2(c)) regions provide sufficient intensity. The peak assignment in Fig. 2 follows the proposal by Inoyatov *et al.* [19] for Cu KLM and Went and Voss [20] for Cu KLL. In this study, the AES peak that shows a strong enough kinetic energy shift for the discrimination of different oxidation states of copper is the Cu $KL_2M_{4,5}$ transition, indicated with an arrow in Fig. 2(c). The lack of strong kinetic energy shifts in the more intense Cu KLL region makes it not possible to use it for the oxidation state determination. A likely explanation to no larger kinetic energy shift in the Cu KLL region is that no Cu 3d ($M_{4,5}$) electrons are participating in the decays, which are involved in the Cu-O bonds and therefore affected by the oxide presence.

In Fig. 3, the AES Cu $L_3M_{4,5}M_{4,5}$ and Cu $KL_2M_{4,5}$ peaks are compared for Cu/Cu_2O(100) (Cu^0), Cu_2O(100) (Cu^+), and CuO/Cu_2O(100) (Cu^{2+}). It is apparent that the two Auger transitions carry similar kinetic energy shifts for the different oxidation states. The gray spectra in Fig. 3(b) show the difference spectra of normalized Cu/Cu_2O(100) and CuO/Cu_2O(100) signals with the normalized Cu_2O(100) signal. Comparing the spectra of Cu_2O(100) and Cu/Cu_2O(100) for the two Auger transitions, it is found that the metallic copper contribution is shifted ~1.7 eV and ~2.2 eV towards higher kinetic energies relative the Cu_2O contribution for Cu $KL_2M_{4,5}$ and Cu $L_3M_{4,5}M_{4,5}$, respectively. It shall be noted that this is the kinetic energy for the measured peak intensity. The smaller observed shift in kinetic energy for the Cu $KL_2M_{4,5}$ peak compared to the Cu $L_3M_{4,5}M_{4,5}$ peak is in part explained by the higher electron kinetic energy and hence the longer electron inelastic mean-free path within the material, meaning that the Cu $KL_2M_{4,5}$ transition permits a deeper probing depth and hence more contribution from the bulk Cu_2O beneath the reduced copper.

A comparison of the AES Cu $L_3M_{4,5}M_{4,5}$ and Cu $KL_2M_{4,5}$ peaks was done by alternatingly measuring the regions during the reduction of Cu_2O(100) to Cu/Cu_2O(100) in 75 mbar H_2 ambient and at 80 °C, the reduction evolution is shown for both Auger transitions side-by-side in Fig. 4. At 75 mbar H_2, the electron scatting in the gas is low enough to permit studying the Cu $L_3M_{4,5}M_{4,5}$ transition and the reduction process progress slow enough to record it gradually for both Auger transitions. The AES Cu $L_3M_{4,5}M_{4,5}$ and Cu $KL_2M_{4,5}$ spectra recorded alternatingly of the reduction process are shown in Fig. 4(a) and (b), the time evolves upwards as indicated by the arrows. To further illustrate the intensity changes in the spectra throughout the reduction process, ΔAES maps are shown in Fig. 4(c) and (d), blue and red colors mean intensity loss and gain, respectively. These ΔAES maps are obtained by subtracting each normalized scan with the normalized initial scan (i.e., Cu_2O(100)). It is apparent for both AES regions that there is an intensity shift towards higher kinetic energies as the reduction of Cu_2O(100) into Cu/Cu_2O(100) proceeds. In attempts to compare the results of using the two Auger transitions to quantitatively determine the amount of signal coming from Cu and Cu_2O, a linear combination of the spectra in Fig. 3 were used to decompose each scan. The results are shown in Fig. 4(e) and (f). The Cu_2O contribution is stronger for AES Cu $KL_2M_{4,5}$ than for AES Cu $L_3M_{4,5}M_{4,5}$, which is explained by the larger information depth caused by the increased electron inelastic mean-free path for electrons with higher kinetic energies. It shall be mentioned again that decreasing the X-ray incidence angle (measured from the surface plane and not surface normal) to more grazing incidence leads to shorter information depth, hence higher surface sensitivity, once the X-ray penetration depth projected onto the surface normal direction is shorter than the electron inelastic mean-free path.

4. Summary and conclusions

This study explores the feasibility of using Auger electron spectroscopy to discern the oxidation states of copper at high gas pressures in hard X-ray electron spectroscopy studies. It is found that the Auger Cu $KL_2M_{4,5}$ transition carries similar information as the Auger Cu $L_3M_{4,5}M_{4,5}$ transition does. The kinetic energy for the peak intensity is significantly larger, ~7935 eV compared to ~914 eV, which leads both to a lower scattering cross-section in the gas phase, this permits studies at higher gas pressures, and to a greater information depth, meaning more contribution from the bulk signal. The information depth can, however, be tuned by the X-ray incidence angle. Furthermore, the energy broadening is larger for the Auger Cu $KL_2M_{4,5}$ transition, which

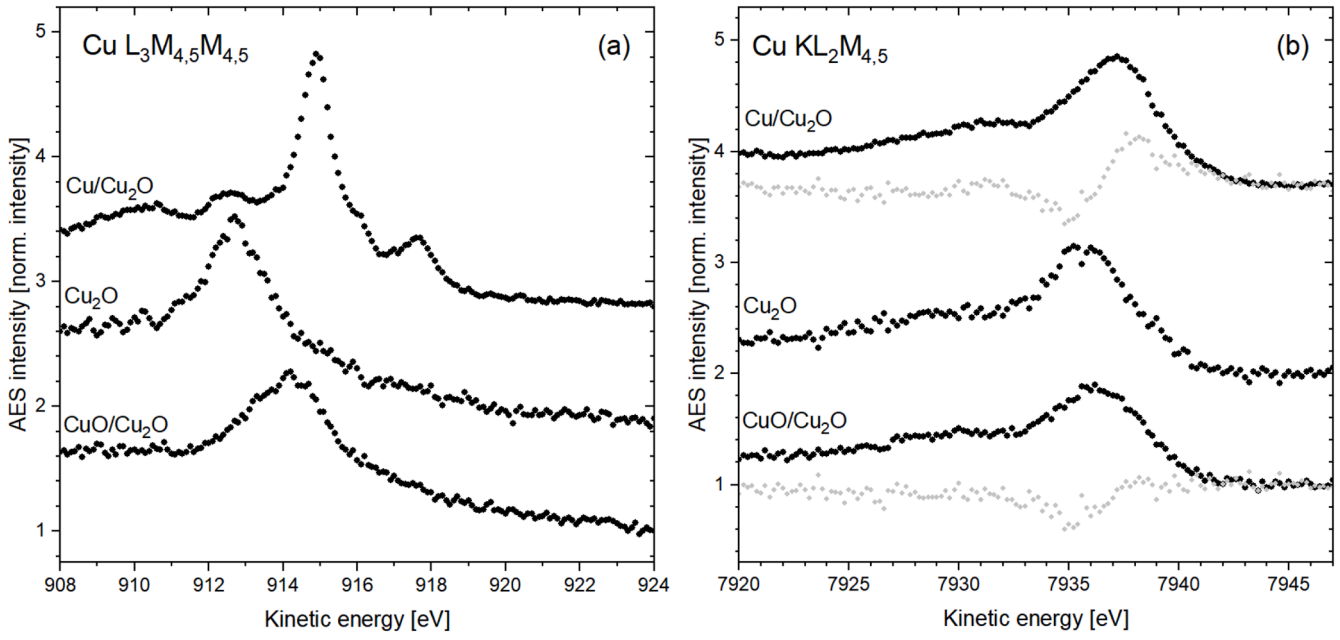


Fig. 3. Auger electron spectra measured at high-vacuum conditions of metallic copper (reduced Cu_2O(100)), Cu_2O(100), and CuO (oxidized Cu_2O(100)). (a) AES Cu $L_3M_{4,5}M_{4,5}$ region. (b) AES Cu $KL_2M_{4,5}$-region. All spectra are normalized on the high-kinetic energy side. The gray spectra in (b) represent the signal difference to Cu_2O.

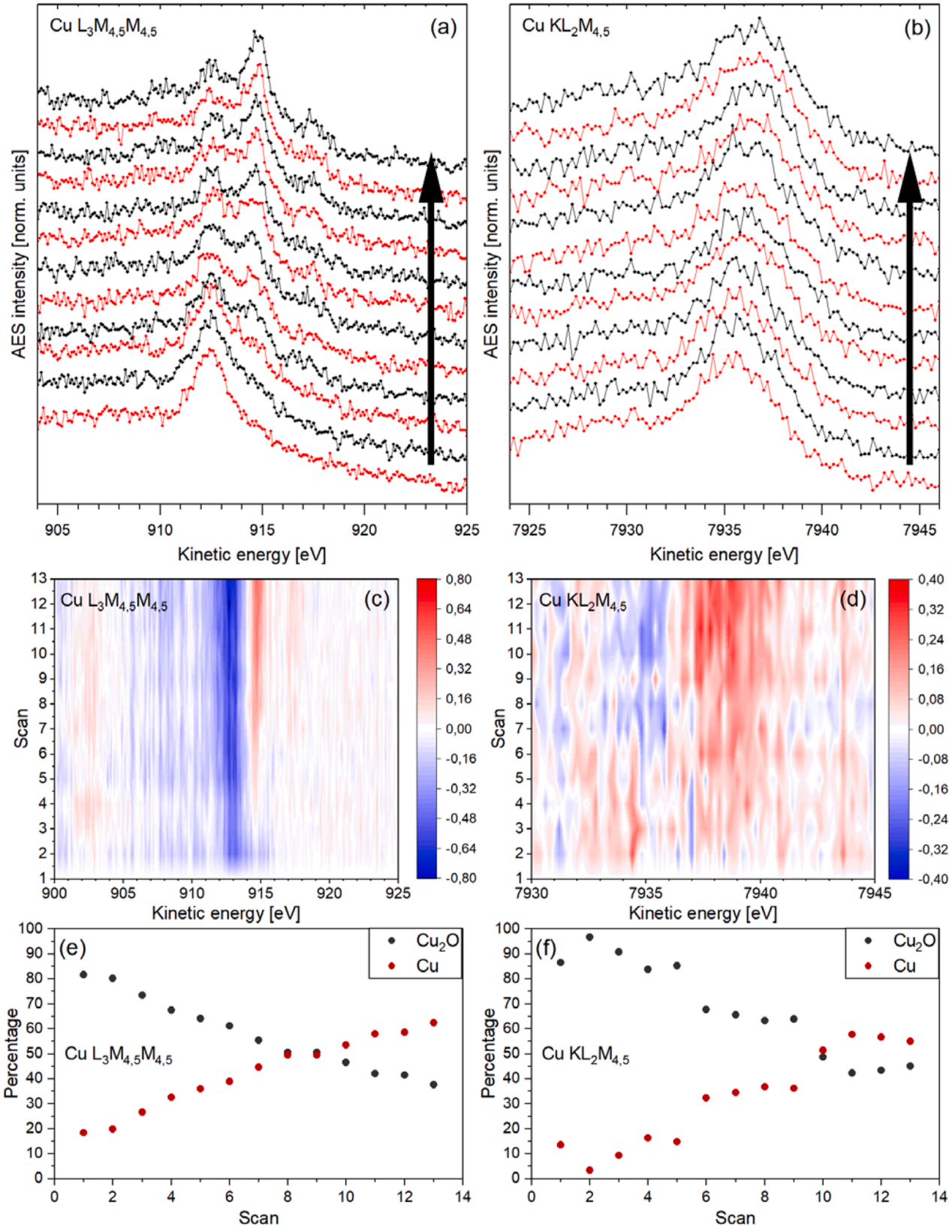


Fig. 4. Auger electron spectra of the Cu $L_3M_{4,5}M_{4,5}$ and Cu $KL_2M_{4,5}$ regions of $Cu_2O(100)$ during reduction in H_2 at 75 mbar and 80 °C. The regions were measured alternating throughout the reduction series. The reduction progress upwards. (a) AES Cu $L_3M_{4,5}M_{4,5}$ (b) AES Cu $KL_2M_{4,5}$ (c) ΔAES Cu $L_3M_{4,5}M_{4,5}$ (d) ΔAES Cu $KL_2M_{4,5}$ (e) and (f) represent percentage contribution of Cu and Cu_2O signal to (c) and (d), respectively.

requires more careful decomposing of the contributions using known reference spectra. The findings suggest it is feasible to utilize the Auger Cu $KL_2M_{4,5}$ transition for oxidation state determination in high-pressure hard X-ray electron spectroscopy studies.

The hard X-ray photoelectron spectra of the Cu 1s core-level follow the pattern from the shallower core-levels. The absence of significant core-level shift makes the discrimination of metallic copper and Cu_2O not feasible. For CuO, the Cu 1s features an additional component on the high-binding energy side of the main peak. The binding energy shift for this component matches the, in literature for shallower core-levels, assigned contribution from core ionization induced electron transfer processes between O 2p- and Cu 3d-states.

CRediT authorship contribution statement

Markus Soldemo: Writing – review & editing, Writing – original draft, Visualization, Supervision, Resources, Project administration, Methodology, Investigation, Funding acquisition, Formal analysis, Data curation, Conceptualization. **Fernando Garcia-Martinez:** Writing – review & editing, Investigation. **Christopher M Goodwin:** Writing – review & editing, Investigation. **Patrick Lömker:** Writing – review & editing, Investigation. **Mikhail Shipilin:** Writing – review & editing, Investigation. **Anders Nilsson:** Writing – review & editing, Resources, Project administration, Funding acquisition. **Peter Amann:** Writing – review & editing, Investigation. **Sarp Kaya:** Writing – review & editing, Investigation. **Jonas Weissenrieder:** Writing – review & editing, Resources, Project administration, Methodology, Investigation, Data curation, Conceptualization.

Declaration of competing interest

The authors declare that they have no known competing financial interests or personal relationships that could have appeared to influence the work reported in this paper.

Data availability

Data will be made available on request.

Acknowledgements

We acknowledge DESY (Hamburg, Germany), a member of the Helmholtz Association HGF, for the provision of experimental facilities. Parts of this research were carried out at PETRA III and we would like to thank Dr. Christoph Schlueter for assistance in using the P22 beamline. Beamtime was allocated for proposal I-20211453. This work was supported by Knut & Alice Wallenberg (KAW) foundation (under grant no. 2016.0042 and 2021.0221) and the Swedish Research Council (under grant no. 2013–8823 and 2021–04379) SSF is acknowledged for financial support within project ITM17–0034. S.K. acknowledges TUBİTAK (Grant number: 118F137). Research by M.S. was supported by the U.S. Department of Energy, Office of Science, Office of Basic Energy Sciences, Chemical Sciences, Geosciences, and Biosciences Division, Catalysis Science Program through the Ultrafast Catalysis FWP 100435 at SLAC National Accelerator Laboratory.

References

[1] B. Eren, C. Heine, H. Bluhm, G.A. Somorjai, M. Salmeron, Catalyst chemical state during CO Oxidation Reaction on Cu(111) studied with ambient-pressure X-ray photoelectron spectroscopy and near edge X-ray adsorption fine structure spectroscopy, J. Am. Chem. Soc. 137 (2015) 11186–11190, https://doi.org/10.1021/jacs.5b07451.

[2] P.B. Rasmussen, P.M. Holmblad, T. Askgaard, C.V. Ovesen, P. Stoltze, J.K. Nørskov, I. Chorkendorff, Methanol synthesis on Cu(100) from a binary gas mixture of CO2 and H2, Catal. Lett. 26 (1994) 373–381, https://doi.org/10.1007/BF00810611.

[3] S. Roy, A. Cherevotan, S.C. Peter, Thermochemical CO2 hydrogenation to single carbon products: scientific and technological challenges, ACS Energy Lett 3 (2018) 1938–1966, https://doi.org/10.1021/acsenergylett.8b00740.

[4] J. Teržan, M. Huš, B. Likozar, P. Djinović, Propylene epoxidation using molecular oxygen over copper- and silver-based catalysts: a review, ACS Catal 10 (2020) 13415–13436, https://doi.org/10.1021/acscatal.0c03340.

[5] Q. Hua, T. Cao, X.-K. Gu, J. Lu, Z. Jiang, X. Pan, L. Luo, W.-X. Li, W. Huang, Crystal-plane-controlled selectivity of Cu_2O catalysts in propylene oxidation with molecular oxygen, Angew. Chem. Int. Ed. 53 (2014) 4856–4861, https://doi.org/10.1002/anie.201402374.

[6] X. Yang, S. Kattel, K. Xiong, K. Mudiyanselage, S. Rykov, S.D. Senanayake, J. A. Rodriguez, P. Liu, D.J. Stacchiola, J.G. Chen, Direct epoxidation of propylene over stabilized Cu^+ surface sites on titanium-modified Cu_2O, Angew. Chem. Int. Ed. 54 (2015) 11946–11951, https://doi.org/10.1002/anie.201504538.

[7] M. Hara, T. Kondo, M. Komoda, S. Ikeda, J.N. Kondo, K. Domen, M. Hara, K. Shinohara, A. Tanaka, Cu2O as a photocatalyst for overall water splitting under visible light irradiation, Chem. Commun. (1998) 357–358, https://doi.org/10.1039/a707440i.

[8] A.E. Baber, X. Yang, H.Y. Kim, K. Mudiyanselage, M. Soldemo, J. Weissenrieder, S. D. Senanayake, A. Al-Mahboob, J.T. Sadowski, J. Evans, J.A. Rodriguez, P. Liu, F. M. Hoffmann, J.G. Chen, D.J. Stacchiola, Stabilization of catalytically active Cu+ surface sites on titanium-copper mixed-oxide films, Angew. Chem. 126 (2014) 5440–5444, https://doi.org/10.1002/ange.201402435.

[9] Applications of X-ray Photoelectron Spectroscopy to Catalytic Studies, WORLD SCIENTIFIC, EUROPE, 2022. https://doi.org/10.1142/q0392.

[10] C. Wang, Y. Kong, M. Soldemo, Z. Wu, H. Tissot, B. Karagoz, K. Marks, J.H. Stenlid, A. Shavorskiy, E. Kokkonen, S. Kaya, D.J. Stacchiola, J. Weissenrieder, Stabilization of Cu2O through site-selective formation of a Co1Cu hybrid single-atom catalyst, Chem. Mater. 34 (2022) 2313–2320, https://doi.org/10.1021/acs.chemmater.1c04137.

[11] Y. Li, H. Chen, W. Wang, W. Huang, Y. Ning, Q. Liu, Y. Cui, Y. Han, Z. Liu, F. Yang, X. Bao, Crystal-plane-dependent redox reaction on Cu surfaces, Nano Res 13 (2020) 1677–1685, https://doi.org/10.1007/s12274-020-2791-z.

[12] K. Roy, C.S. Gopinath, UV photoelectron spectroscopy at near ambient pressures: mapping valence band electronic structure changes from Cu to CuO, Anal. Chem. 86 (2014) 3683–3687, https://doi.org/10.1021/ac4041026.

[13] M. Li, T.H.M. Pham, E. Oveisi, Y. Ko, W. Luo, A. Züttel, Revealing the surface chemistry for CO2 hydrogenation on Cu/CeO2–x using near-ambient-pressure X-ray photoelectron spectroscopy, ACS Appl. Energy Mater. 4 (2021) 12326–12335, https://doi.org/10.1021/acsaem.1c02146.

[14] J. Wang, C. Li, Y. Zhu, J.A. Boscoboinik, G. Zhou, In Situ monitoring of H2-Induced Nonstoichiometry in Cu_2O, J. Phys. Chem. Lett. 13 (2022) 5597–5604, https://doi.org/10.1021/acs.jpclett.2c00988.

[15] A. Regoutz, G. Kerherve, I. Villar-Garcia, C.K. Williams, D.J. Payne, The influence of oxygen on the surface interaction between CO2 and copper studied by ambient pressure X-ray photoelectron spectroscopy, Surf. Sci. 677 (2018) 121–127, https://doi.org/10.1016/j.susc.2018.06.004.

[16] N. Pauly, S. Tougaard, F. Yubero, LMM Auger primary excitation spectra of copper, Surf. Sci. 630 (2014) 294–299, https://doi.org/10.1016/j.susc.2014.08.029.

[17] C. Nordling, E. Sokolowski, K. Siegbahn, Precision method for obtaining absolute values of atomic binding energies, Phys. Rev. 105 (1957) 1676–1677, https://doi.org/10.1103/PhysRev.105.1676.

[18] D.H. Lee, B.M. Johnson, N.A. Guardala, J.L. Price, G.A. Glass, M.F. Stumborg, K. W. Jones, Ar Ne, Fe, and Cu auger-electron production at national synchrotron light source, Nucl. Instrum. Methods Phys. Res. Sect. B Beam Interact. Mater. At. 79 (1993) 261–264, https://doi.org/10.1016/0168-583X(93)95339-7.

[19] A.Kh. Inoyatov, L.L. Perevoshchikov, V.S. Zhdanov, D.V. Filosofov, A. Kovalík, Experimental KLM+KLN Auger spectrum of Cu, J. Electron Spectrosc. Relat. Phenom. 189 (2013) 23–26, https://doi.org/10.1016/j.elspec.2013.06.003.

[20] M.R. Went, M. Vos, Electron-induced KLL Auger electron spectroscopy of Fe, Cu and Ge, J. Electron Spectrosc. Relat. Phenom. 148 (2005) 107–114, https://doi.org/10.1016/j.elspec.2005.04.004.

[21] S. Egri, L. Kövér, I. Cserny, M. Novák, W. Drube, Analysis of KLL Auger spectra excited by X-rays from Ni and Cu metal surfaces, Photon Fast Ion Induc. Process. At. Mol. Nanostruct. PIPAMON 369 (2016) 15–20, https://doi.org/10.1016/j.nimb.2015.10.027.

[22] H. Tissot, C. Wang, J.H. Stenlid, T. Brinck, J. Weissenrieder, The surface structure of Cu2O(100): nature of defects, J. Phys. Chem. C 123 (2019) 7696–7704, https://doi.org/10.1021/acs.jpcc.8b05156.

[23] M. Soldemo, J.H. Stenlid, Z. Besharat, M. Ghadami Yazdi, A. Önsten, C. Leygraf, M. Göthelid, T. Brinck, J. Weissenrieder, The surface structure of Cu2O(100), J. Phys. Chem. C 120 (2016) 4373–4381, https://doi.org/10.1021/acs.jpcc.5b11350.

[24] K.H. Schulz, D.F. Cox, Photoemission and low-energy-electron-diffraction study of clean and oxygen-dosed ${\mathrm{Cu}}_{2}$O (111) and (100) surfaces, Phys. Rev. B 43 (1991) 1610–1621, https://doi.org/10.1103/PhysRevB.43.1610.

[25] K.H. Schulz, D.F. Cox, Surface hydride formation on a metal-oxide surface - the interaction of atomic-hydrogen with Cu2O(100), Surf. Sci. 278 (1992) 9.

[26] H. Tissot, C. Wang, J.H. Stenlid, M. Panahi, S. Kaya, M. Soldemo, M. Ghadami Yazdi, T. Brinck, J. Weissenrieder, Interaction of atomic hydrogen with the Cu2O (100) and (111) surfaces, J. Phys. Chem. C 123 (2019) 22172–22180, https://doi.org/10.1021/acs.jpcc.9b03888.

[27] T.A. Ramanarayanan, J. Alonzo, Oxidation of copper and reduction of Cu2O in an environmental scanning electron microscope at 800°C, Oxid. Met. 24 (1985) 17–27, https://doi.org/10.1007/BF00659595.

[28] P. Amann, D. Degerman, M.-T. Lee, J.D. Alexander, M. Shipilin, H.-Y. Wang, F. Cavalca, M. Weston, J. Gladh, M. Blom, M. Björkhage, P. Löfgren, C. Schlueter, P. Loemker, K. Ederer, W. Drube, H. Noei, J. Zehetner, H. Wentzel, J. Åhlund, A. Nilsson, A high-pressure x-ray photoelectron spectroscopy instrument for studies of industrially relevant catalytic reactions at pressures of several bars, Rev. Sci. Instrum. 90 (2019) 103102, https://doi.org/10.1063/1.5109321.

[29] C. Schlueter, A. Gloskovskii, K. Ederer, I. Schostak, S. Piec, I. Sarkar, Yu. Matveyev, P. Lömker, M. Sing, R. Claessen, C. Wiemann, C.M. Schneider, K. Medjanik, G. Schönhense, P. Amann, A. Nilsson, W. Drube, The new dedicated HAXPES beamline P22 at PETRAIII, AIP Conf. Proc 2054 (2019) 040010, https://doi.org/10.1063/1.5084611.

[30] B.L. Henke, E.M. Gullikson, J.C. Davis, X-Ray interactions: photoabsorption, scattering, transmission, and reflection at E = 50-30,000 eV, Z = 1-92, At, Data Nucl. Data Tables 54 (1993) 181–342, https://doi.org/10.1006/adnd.1993.1013.

[31] K.H. Schulz, D.F. Cox, Photoemission and low-energy-electron-diffraction study of clean and oxygen-dosed Cu2O (111) and (100) surfaces, Phys. Rev. B 43 (1991) 1610–1621, https://doi.org/10.1103/PhysRevB.43.1610.

[32] C. Wang, H. Tissot, C. Escudero, V. Pérez-Dieste, D. Stacchiola, J. Weissenrieder, Redox properties of Cu_2O(100) and (111) surfaces, J. Phys. Chem. C 122 (2018) 28684–28691, https://doi.org/10.1021/acs.jpcc.8b08494.

[33] P.A.W. van der Heide, Multiplet splitting patterns exhibited by the first row transition metal oxides in X-ray photoelectron spectroscopy, J. Electron Spectrosc. Relat. Phenom. 164 (2008) 8–18, https://doi.org/10.1016/j.elspec.2008.04.001.

[34] P.S. Miedema, F. Borgatti, F. Offi, G. Panaccione, F.M.F. De Groot, Iron 1s X-ray photoemission of Fe2O3, J. Electron Spectrosc. Relat. Phenom. 203 (2015) 8–13, https://doi.org/10.1016/j.elspec.2015.05.003.

[35] O. Karis, S. Svensson, J. Rusz, P.M. Oppeneer, M. Gorgoi, F. Schäfers, W. Braun, W. Eberhardt, N. Mårtensson, High-kinetic-energy photoemission spectroscopy of Ni at 1s : 6-eV satellite at 4 eV, Phys. Rev. B 78 (2008) 233105, https://doi.org/10.1103/PhysRevB.78.233105.

[36] A. Önsten, J. Weissenrieder, D. Stoltz, S. Yu, M. Göthelid, U.O. Karlsson, Role of defects in surface chemistry on Cu2O(111), J. Phys. Chem. C 117 (2013) 19357.

[37] H.-Y. Wang, M. Soldemo, D. Degerman, P. Lömker, C. Schlueter, A. Nilsson, P. Amann, Direct evidence of subsurface oxygen formation in oxide-derived Cu by X-ray photoelectron spectroscopy, Angew. Chem. Int. Ed. 61 (2022) e202111021, https://doi.org/10.1002/anie.202111021.

[38] J.H. Stenlid, M. Soldemo, A.J. Johansson, C. Leygraf, M. Göthelid, J. Weissenrieder, T. Brinck, Reactivity at the Cu_2O(100):Cu–H_2O interface: a combined DFT and PES study, Phys. Chem. Chem. Phys. 18 (2016) 30570–30584, https://doi.org/10.1039/C6CP04410G.